Int. J. Heat Mass Transfer. Vol. 35, No. 12, pp. 3237–3244, 1992
Printed in Great Britain

0017–9310/92 $5.00 + 0.00

Marangoni–Bénard instabilities under non-steady conditions. Experimental and theoretical results

O. DUPONT,† M. HENNENBERG‡ and J. C. LEGROS†

† Université Libre de Bruxelles, Microgravity Research Centre, CP. 165, Av. F. D. Roosevelt, 50, 1050 Brussels, Belgium

‡ Université Libre de Bruxelles, Service de Chimie Physique, CP. 231, Boulevard du Triomphe, 1050 Brussels, Belgium

(*Received* 8 *October* 1991 *and in final form* 25 *February* 1992)

Abstract—The onset of Marangoni–Bénard instability under microgravity conditions is studied experimentally using a sounding rocket (TEXUS 21) launched in the microgravity program developed by the European Space Agency. Due to the short available time, the experiment is conducted under unsteady conditions, i.e. the temperature gradient inside the liquid phase is not constant. For such a non-linear temperature profile, we compare the experimental and the theoretical value of the critical non-oscillatory Marangoni number. This simple analysis provides an excellent agreement in contradistinction with earlier results obtained during Apollo 14 and 17 flights.

1. INTRODUCTION

PEARSON [1] reviewing the original Bénard [2] experiments done in thin liquid layers heated from the rigid bottom side, pointed out that the onset of cellular convection was obtained outside of the theoretical frame put forward in Lord Rayleigh's [3] classical article. There, convection will appear, once the effects of buoyancy due to liquid thermal expansion, overcome the dissipative effects of bulk viscosity and heat diffusivity. These experimental situations corresponded to cases where convective hexagonal Bénard cells are observed, even if the buoyancy effects are small and remain ineffective. This was so since Marangoni stresses at the free interface are the leading cause behind those selected structures. For a constant temperature gradient, Nield [4] compared the relative effects of buoyancy and surface tension on the onset of instability. His theoretical model was substantiated by Harvey *et al.*'s [5] experiments which enable us to compare with a rather good approximation various hypothetical situations to practical ones.

One very important issue was then raised: how to describe the onset of convection due to surface effects whenever the temperature profile is far from a steady linear one. Vidal and Acrivos [6] considered already the problem in shallow evaporating pools of propyl alcohol. They proposed a way to find out the critical Marangoni number in the absence of buoyancy effects and compared their numerical value to the one which they deduced from an experiment on earth. Still, they recorded a discrepancy between theoretical and experimental results which they attributed to the use of the selected profile and to buoyancy.

Experiments, with a concentration dependent Marangoni effect, were also performed during the Spacelab D1 mission, with a flat liquid–gas interface. Unhappily, no convective instability has been recorded (cf. the experiment of Lichtenbelt *et al.* [7]).

Thus, instability conditions for such cases require a careful study in a real microgravity environment, where one could compare the experimental and the theoretical values of the Marangoni number. Such experiments were already done during the Apollo program [8–11]. Despite technical difficulties which had to be overcome and severe experimental drawbacks, it was shown beyond doubt that surface tension gradients alone are sufficient to induce convective motions. This was not experimentally proven before. The motion starts when the temperature drop inside the liquid layer exceeds a critical value. Also a polygonal cellular pattern is preferred to roll cells.

But, despite these rewarding results, important items remained pretty obscure. The experimentally deduced Marangoni numbers were larger than the ones predicted from Pearson's theoretical approach [1], whatever the thermal behaviour of the liquid–gas interface. The critical temperature difference increases when the depth of the fluid layer is increased. This behaviour was also observed by Koschmieder [12] on thin layers heated from below, when the surface tension effects are dominant. Experimental results under microgravity conditions are thus far from being completely understood. Furthermore, a basic methodological difficulty had to be overcome: one cannot take into account any more just Pearson's model for the temperature profile. Indeed Pearson supposes the steady reference state to correspond to a constant temperature gradient across the liquid layer at rest. This can be experimentally so after a long time as was

NOMENCLATURE

a_i	polynomial coefficient of the transient temperature profile ($i = 1, 2, 3$)
B	Biot number
d	liquid depth
k	heat conductivity
K	thermal diffusivity
Ma	Marangoni number
S	surface tension
T	temperature
T_{0s}	free surface temperature
ΔT	temperature difference across the liquid layer.

Greek symbols

α	wave number
μ	dynamic viscosity
ξ	adimensional length along z axis
ρ	density
σ	temperature dependence of S.

stated explicitly by Harvey *et al.* [5] who needed a certain number of hours to reach it. These conditions are excluded inside the 6 min provided by the ballistic path of a sounding rocket.

The present paper reports a Marangoni–Bénard experiment using the specific microgravity amenities of the TEXUS 21 sounding rocket flight performed in the frame of the microgravity program of ESA. During the finite span of time available, we were only able to observe the transient behaviour of the heating process. Even though, we suppose in this first report, a quasi steady temperature profile, its spatial shape is strongly nonlinear and we develop a linear stability analysis to describe the marginal non-oscillating neutral state, neglecting for the time being, the free surface deformation. For that case, the numerical analysis gives the theoretical values of the critical Marangoni number and the Biot number which are favourably compared to their experimental values since they fall inside the experimental error interval.

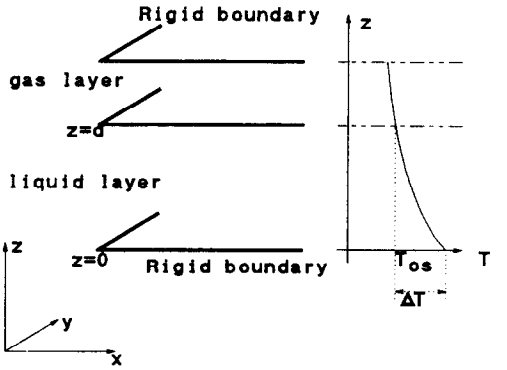

FIG. 1. Schematic view of the experiment and an example of the temperature distribution in the liquid and gas phases.

2. MATHEMATICAL FORMULATION

Let us consider an infinite liquid layer bounded on the one side by a horizontal rigid wall at $z = 0$ and, on the other side by a horizontal free liquid–gas interface at $z = d$. The experimental constraints and procedures that we have to follow inboard the rocket during this Spacelab precursor flight, exclude the necessary facilities to get the transition from a quiescent conducting liquid to the convective Bénard cells by departing, infinitely slowly from one linear temperature profile to another.

But in the allotted time, the heating processing which we describe elsewhere [13], enables us to represent our experimental data with a high degree of accuracy by a quasi steady profile which shows a spatial dependency on the form of a cubic equation:

$$T = T_{0s} + a_1(z-d) - a_2(z-d)^2 - a_3(z-d)^3 \quad (1)$$

where T_{0s} is the temperature at the free interface. The profile is frozen with respect to time (see Fig. 1). Obviously, this last hypothesis means that this equation rests on a compromise. It might not be very gratifying for other purposes. But, this empirical shape has kept the most important feature of the transient conducting profile, which we want to tackle with: namely its curvature is finite and changes continuously with height (see Fig. 2). Since all our data derive only from microgravity, this constitutes a major difference with Vidal and Acrivos [6] who applied Currie's [14] approach.

Adopting equation (1) for a reference profile, we

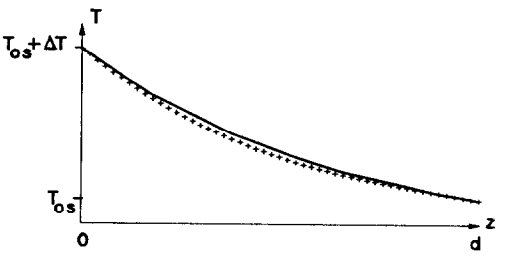

FIG. 2. Comparison between the temperature distribution in the liquid obtained from the numerical calculation (+) and a polynomial of the third degree corresponding to the onset of convection (continuous line).

study the linear stability of the corresponding thermocapillary problem in the absence of gravity and determine the onset of convection for an undeformable interface. The unperturbed profile does not obey Fourier's equation but the fluctuations of temperature T' do so. Thus, we follow stepwise the general linear perturbation scheme in the absence of buoyancy put forward by Pearson, adopting his nomenclature and adimensionalization wherever possible and referring the reader to his article for more details [1]. Let us stress that the temperature is scaled by the total temperature drop across the layer ΔT, given by

$$\Delta T = a_1 d - a_2 d^2 + a_3 d^3. \tag{2}$$

To study the marginal stationary stability of infinitesimal disturbances, one decomposes them into a Fourier integral expansion along the plane parallel to the non-deformed free surface. This standard procedure algebrizes the whole problem with respect to the x/d and y/d variables. The whole mathematical difficulty becomes now the study of a time independent system of ordinary differential equations in the dimensionless variable $\xi = z/d$ for only one single mode defined by α, the dimensionless wave number.

Along the undeformable liquid–gas surface, the tangential shear stress of the liquid layer is balanced by the longitudinal variation of the surface tension S which decreases linearly with temperature. This introduces a coupling between the heat and the momentum, both being taken along the free interface

$$S = S_0 - \sigma T \tag{3}$$

where the rate of heat loss per unit area obeys Newton's cooling law. This defines the heat of transfer coefficient q. It expresses the loss of heat into the gaseous adjacent phase $(qdT')_s$ to be equal to the heat flux coming from the liquid. This last is given by Fourier's law—$k(\partial T'/\partial \xi)$ and thus introduces the coefficient k of heat conduction in the liquid.

At the rigid wall, there is no slip and we consider the limiting case of a heat conducting wall, thus $T' = 0$. This boundary condition corresponds to rather ad hoc situations and is actually an extension of the properties of the real device which we used in our microgravity experiment.

We have now to solve the following system of coupled differential equations linking the velocity component $f(\xi)$ of the normal mode and the temperature perturbation component $g(\xi)$ of the normal mode:

$$(D^2 - \alpha^2)^2 f(\xi) = 0 \tag{4}$$

$$(D^2 - \alpha^2) g(\xi) = f[a_1^* + 2a_2^*(\xi - 1) + 3a_3^*(\xi - 1)^2] \tag{5}$$

where $D = d/d\xi$ and

$$a_i^* = \frac{a_i d^i}{\Delta T}. \tag{6}$$

The boundary conditions related to our problem are

$$f(0) = f'(0) = 0, \quad f(1) = 0, \quad f''(1) = \alpha^2 \, Ma \, g(1)$$

$$Ma = \frac{\sigma \Delta T d}{K\mu}, \quad g'(1) = -Bg(1)$$

$$B = \frac{qd}{k}, \quad g'(0) = 0. \tag{7a–g}$$

Equation (4) is deduced from the expansion of the Navier–Stokes equation and equation (5) corresponds to the heat equation. We study, here, only the neutral stationary state. This specific case is independent from the Prandtl number as is well known from standard studies [1, 4, 7]. It is evident that any analysis of a more general character should show the influence of this parameter as it will intervene at least on the frequency of the oscillatory motion. Also, we limit ourselves to the onset of steady convection, we are not yet considering finite motion. This is why we neglect also the surface deformation. The right-hand side of equation (5) is due to the convective transport of heat whose unperturbed profile is given by equation (1).

The dimensionless number Ma defined by equation (7d) is the equivalent of a Reynolds number. It expresses thus that motion will be induced by surface forces and opposed by viscous and thermal dissipation. The Biot number B characterizes the heat exchange at the discontinuous liquid–gas interface. From equations (4), (7a) and (7b), one finds directly the explicit expression for $f(\xi)$. Up to an unknown constant factor r, it is given by

$$f(\xi) = r\left(\sinh \alpha\xi + \frac{\alpha \cosh \alpha - \sinh \alpha}{\sinh \alpha} \xi \sinh \alpha\xi - \alpha\xi \cosh \alpha\xi\right). \tag{8}$$

It is the same solution as the one given by Pearson, for an undeformable surface. This is a consequence of the microgravity environment which eliminates any coupling between the Navier–Stokes momentum balance and heat since there is no external volumic force linked to heat; due to the experimental working conditions, the onset of motion is driven solely by the free surface longitudinal variations. One introduces the above expression for $f(\xi)$ in equation (5) which becomes thus a second order inhomogeneous ordinary differential equation with constant coefficients. In the appendix, we give the explicit solution for the thermally conducting rigid wall ($g(0) = 0$) which corresponds to our experimental situation.

We have obtained the complete expressions of the solutions for both $f(\xi)$ and $g(\xi)$. Calculating the two components of the mode at $\xi = 1$, we use the boundary condition (7c) to derive the compatibility condition of this problem, so that every physical perturbation will be defined, once the value of the amplitude

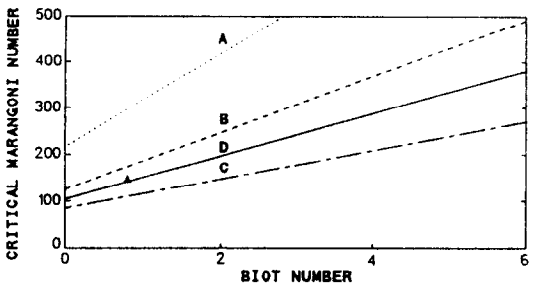

FIG. 3. Critical Marangoni number vs Biot number for the case: curve A, $a_3^* = 1$; curve B, $a_2^* = 1$; curve C, $a_1^* = 1$ (Pearson's theory); curve D, experimental conditions at the onset ($a_1^* = 0.6$, $a_2^* = 0$, $a_3^* = 0.34$). The experimental value is noted as ▲.

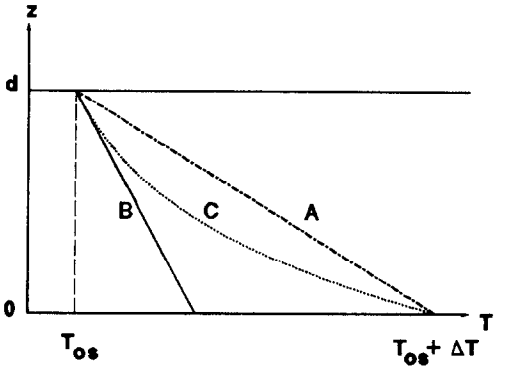

FIG. 4. Comparison between various profiles. Curve A, linear, the ΔT across the layer is equal to the one of curve C; curve B, linear, the gradient of T at the free surface is equal to the one of curve C; curve C, cubic profile.

r is given. We obtain the functional form of Ma, as a function of the Biot number B, the wave number α and any two of the three parameters a_i^*. Indeed there exists a linear dependency between those three parameters since by definition, one has

$$a_1^* - a_2^* + a_3^* = 1 \tag{9}$$

so that the whole discussion is now on the function

$$Ma = Ma(\alpha, B, [a_i^*, i \in (1, 3)]). \tag{10}$$

Thus, for each set of the control parameters B and a_i^* ($i = 1, 2, 3$) we derive from equation (10), a curve giving the Marangoni number, Ma, in terms of the wave number α whose minimal value is the critical Marangoni number Ma_c, which is the most interesting quantity of our problem. For example this numerical procedure gives us back the Pearson value since for $a_1^* = 1$ we obtained $Ma_c = 79.6$ with $\alpha = 2.0$ for a thermally conducting rigid wall. From a comparison of numerical simulations, we extract also the Ma_c as a function of the Biot number at $a_2^* = -1$ and $a_3^* = 1$, which we compare with the experimental values of the Biot and the Marangoni numbers (see Fig. 3).

Let us consider the linear temperature drop whose limiting values across the liquid layer are equal to the ones being observed on the two boundaries. This situation is depicted with the curve A in Fig. 4. For the same temperature drop ΔT, our cubic profile (see curve C, Fig. 4) still gives us a certain freedom on the choice of a_i^* coefficients, and thus on the shape of the profile. As the curvature, in our experiment as well as in the one performed by Grodzka and Bannister [8–11] is positive, the temperature at the same height in the liquid is always smaller for a cubic profile than for a linear one. Thus, to reach a convective regime one must provide a stronger cause for the instability and Ma_c will increase with a_3^* or a_2^*. To illustrate this, let us change a_1^*, at the same temperature drop ΔT. This amounts to varying the value of the reference temperature gradient at the free surface and implies to study another Marangoni curve as the right-hand side of equation (10) shows.

Another point of view is that we consider the same value as Pearson for the gradient of temperature measured at the free liquid–gas interface, which is kept at one temperature (see curve B, Fig. 4). Then, an equivalent approach would be to define as the total linear temperature drop ΔT

$$\Delta T_{\text{Pearson}} = a_1 d \tag{11}$$

so that one has

$$a_1^* = \frac{\Delta T_{\text{Pearson}}}{\Delta T}. \tag{12}$$

This means physically that, in all cases for which a_1^* is smaller than one, the temperature at the rigid solid–liquid surface should be higher than the one which Pearson would consider since the tangent at the free surface leaves the cubic profile at its right (see Fig. 4). At the same height in the liquid, we are now above the linear temperature profile given by equation (11). Now, let us compare two linear profiles, the first corresponding to our actual ΔT and the other for $\Delta T_{\text{Pearson}}$, we have since a_1^* is smaller than 1. But this is a fortiori even more true

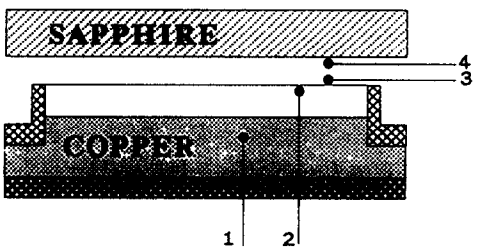

FIG. 5. Sketch of the cell module launched in TEXUS 21. The temperature sensors are noted respectively as 1, 2, 3, 4. Temperature thermistor 2 is located in the silicone oil and sensors 3 and 4 are in the helium layer.

$$\frac{\sigma \Delta T_{\text{Pearson}}}{\mu K} \leqslant \frac{\sigma \Delta T}{\mu K}$$

for the cubic profile corresponding to ΔT, for which the marginal state is reached at an even larger Marangoni number, as we discussed above. As equation (10) which defines the onset of convective instability is a dimensionless equation in terms of dimensionless parameters, both interpretations are valid. Moreover, it is natural to get again Pearson results from equation (10), since for a constant temperature gradient across the whole liquid layer there is only one Marangoni number. It corresponds to

$$Ma = Ma(\alpha, B, a_1^* = 1, a_2^* = a_3^* = 0). \quad (13)$$

3. EXPERIMENTAL DESCRIPTION AND RESULTS

Our main goal is to develop the study of the Marangoni instability under microgravity conditions in a well defined experiment. This means that, we have to satisfy a certain number of criteria which are specific of the spacecraft working conditions and amenities. The main points of concern are linked to the available limited mass, energy and volume budget in a stockpiled sounding rocket and to the finite time during which the desired microgravity level can be sustained. Thus, we must design a way to control and record the temperature at an exactly defined interface, inside a containing vessel whose shape and physico-chemical own properties should not intervene to obscure the interpretation of the data.

Also, one difficulty encountered in microgravity research applied to fluid hydrodynamics, is to obtain a well-defined liquid–gas interface shape: in our present case a large flat interface. In previous experiments [8–11], the free interface showed a curvature, thus introducing thermal gradients along the surface. This experimental feature was casting some very strong doubts on the physical interpretation of the quantitative values.

In short, we want to measure the critical Marangoni number at the onset of convection but we are not allowed to follow the transition from pure heat conduction to thermal convection under conditions which correspond to a quasi steady state. The experimental working conditions exert a heavy toll. One must find a compromise between all these experimentally linked contingencies. One is led to develop specific microgravity relevant experimental techniques [13, 15].

Thus, we considered a rectangular cell whose cross section was 40×60 mm. Its depth was 10 mm out of which the first 5 mm were filled with a silicone oil 200 DC whose characteristics are given in Table 1. The depth of the silicone layer has been carefully selected. The relaxation time of the silicone oil layer d^2/K is about 300 s. This is of the order of magnitude of the total span of time during which the sounding rocket is in a microgravity regime. Helium gas filled the other 5 mm deep half cell. The side walls were in Lexan whose thermal characteristics are close to those of the silicone oil to eliminate as best as possible lateral thermal gradients which could induce motions by themselves.

The hot rigid wall beneath the oil is a copper block, which is heated right after the liquid injection in the cell. The copper high thermal conductivity ensures isothermal conditions but the block is sufficiently thin to allow a quick heating. The other wall, above the gaseous phase, is colder than the copper one. It is a sapphire window giving the opportunity to combine its thermal properties and its optical transparency to visualize the onset of convection (see Table 2). The silicone oil is seeded with aluminium flakes whose reflectivity will outline the convective pattern.

The heat conductivities of the silicone oil and of the helium gas are very near one to another, but their heat diffusivities are in a ratio that largely exceeds 10^3 (see Table 1). The helium large thermal diffusivity and conductivity make sure that the temperature difference, between the liquid interface and the sapphire wall, leaves a reasonable temperature drop across the entire system and that the relaxation time inside the gaseous phase is sufficiently short. The choice of helium has thus a double advantage. It is reasonable to assume a linear temperature gradient in the gaseous phase. Furthermore, since there is no heat accumulation at the interface, the temperature and its normal gradient are continuous along the border separating the oil and the helium.

To follow the heating process, we placed four temperature thermistors in the system. The first one is located in the copper block which is a thermally good conductor. The second and third ones are just below and above the free silicone oil/helium interface. The last one is below the sapphire interface. The sensors have been selected to be as thin as possible to avoid detrimental effects induced by their shape so that the wires have a radius of 0.025 mm and their heads have a 0.4 mm diameter. They allow the measurement of the heat flux crossing both the liquid and the gas layers.

We adapted the Schmidt–Milverton plotting technique [16] to detect the onset of the convective instability and to determine the critical Marangoni number. At the critical point, the slope is changing, due to the appearance of a new mechanism in heat transport. The temperature drop in the oil as a function of the temperature drop in the gas are two different linear functions (in a first approximation). The interaction of the two straight lines defines accurately the onset of convective motion.

The temperature drops related to the onset of convection are

$$\Delta T_{\text{oil}} = 8.9\ \text{K} \pm 0.2\ \text{K}; \quad \Delta T_{\text{Helium}} = 6.1\ \text{K} \pm 0.2\ \text{K} \quad (14)$$

across each of the corresponding 5 mm thick layers

Table 1. Properties of liquids and gas used

Properties	Silicone oil 200 DC	Helium
Dynamic viscosity, μ (kg m^{-1} s^{-1})	14.5×10^{-2}	—
Density, ρ (kg m^{-3})	965	17.8×10^{-2}
Thermal conductivity, k (W K^{-1} m^{-1})	15.5×10^{-2}	15.2×10^{-2}
Surface tension, S (N m^{-1})	21×10^{-3}	—
Temperature dependence of S, σ (N m^{-1} K^{-1})	-5×10^{-5}	—
Thermal diffusivity, K (m^2 s^{-1})	11.3×10^{-8}	84.5×10^{-5}

Table 2. Properties of materials used

Properties	Copper	Lexan	Sapphire
Thermal conductivity, k (W K^{-1} m^{-1})	399	0.19	10
Thermal diffusivity, K (m^2 s^{-1})	11.5×10^{-5}	1.3×10^{-7}	20.9×10^{-7}

tions (7d) and (14) give us the experimental value of the critical Marangoni number

$$Ma_c = 144\pm3.$$

To compare with a theoretical value, we will first evaluate the right-hand side of equation (10). We derive from a least square fitting the polynom which is the nearest to the temperature profile obtained, with the help of a numerical simulation (see Fig. 2), from the heat sensors data. We observe that a cubic approximation is a suitable choice which justifies equation (1) and as a consequence the analytical development giving rise to equation (10). As the thermal gradient is constant in the helium phase and as the heat fluxes are equal along the free interface, we obtain, from equation (14), the linear term and the values of the other coefficients a_i of the polynomial approximation given by equation (1) for the silicone oil layer and obtain

$$a_1 = 1173\ \text{K m}^{-1};\quad a_2 = 0\ \text{K m}^{-2};$$
$$a_3 = 2.42\times10^7\ \text{K m}^{-3}. \qquad (15)$$

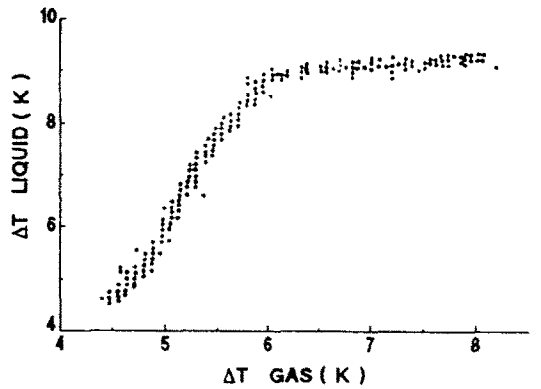

FIG. 6. Schmidt–Milverton plot showing the temperature drop in oil vs temperature drop in the gas layer. The break in the curve gives the ΔT at the onset of convection.

Table 3. Values of the critical Marangoni numbers for the present theory, for the Pearson work and deduced from the experimental data, at different values of the Biot number Bi

Bi	Ma_{exp}	Ma_{theory}	$Ma_{Pearson}$
0.6	—	130.5	101.8
0.8	144 ± 3	139.9	109.0
1.1	—	153.7	119.6

To achieve our goal, we also need to evaluate the Biot number $B = qd/k$ at $T = T_{0s}$, and we will replace q by a finite difference with respect to time, again playing on the assumption of a linear heat profile in the helium phase

$$B = \frac{Q_{t1}-Q_{t2}}{T_{0s(t1)}-T_{0s(t2)}}\frac{d_{oil}}{k_{oil}} \qquad (16)$$

$$B = \frac{\Delta T_{t1}-\Delta T_{t2}}{T_{0s(t1)}-T_{0s(t2)}}\frac{d_{oil}}{k_{oil}}\frac{k_{He}}{d_{He}} \qquad (17)$$

where all the quantities are measured at time $t1$ and $t2$ separated by 10 s. From this, we find a Biot number varying between 0.6 and 1.1 with a mean value of 0.8. Introducing those values in equation (10), we obtain finally a critical Marangoni number equal to 139.9 (see Table 3). It should be also compared to the same quantity deduced from Pearson's model which gives us $Ma_c = 109$ for $B = 0.8$. We notice thus a great improvement as our value is in the error range of the experimental one while the one deduced from Pearson's model is much too low (see Table 3).

4. CONCLUSIONS

Our justification of the present research is to explain why the critical Marangoni number measured at the onset of convection in previous weightlessness experiments is much too high. One of the mean specific experimental features overlooked in the Apollo mission [8–11] was to control the liquid–gas interface shape during the whole of the available time and to carefully determine the onset of convective instability induced by variation of surface tension only for a transient conducting profile of temperature. We succeeded in mastering one very important technical difficulty: we make it possible to fill the half cell in weightlessness, to create and maintain a large flat liquid–gas interface in the timespan during which a

microgravity regime exists. We performed a Marangoni–Bénard experiment in the TEXUS 21 sounding rocket experiment launched in Kiruna on 21 May 1989 and followed the onset of convection in a liquid layer of well defined thermal properties, subject to a transverse non-uniform thermal gradient, and whose containing vessel has well known thermophysical, wetting and geometrical characteristics. This was an important preliminary condition to be fulfilled to successfully perform a microgravity experiment during the Spacelab D2 Mission in 1992.

Then, taking those experimental conditions into consideration, we reformulate the linear stability problem for thermocapillary convection in weightlessness, induced by a transient temperature profile. It is thus different from the linear one studied by Pearson and we assimilated it to a quasi steady state since its relaxation time is of the order of magnitude of the microgravity lifetime. The conducting temperature reference profile was evaluated by a cubic polynomial which has a continuously varying curvature with height.

We report in this paper the critical Marangoni number at the onset of convection induced by such a quasi steady temperature profile and reach an excellent agreement with the experimental results. This illustrates an obvious methodological point: a theory which should be applied within the framework of space facilities has to incorporate the specific microgravity experimental conditions at hand and be compared to experimental results.

Acknowledgements—The TEXUS microgravity experiment was accepted and launched by ESA and the basic research at U.L.B. was supported by ESA Prodex contract, an 'Action de Recherche Concertée' convection from Belgian Science Policy Office and a 'Fonds de la Recherche Fondamentale Collective' contract. The μg TEXUS experiment was contracted and built by the MBB-ERNO-TEXUS Team. The experiment was supported by a NATO group (contract No. 916/83).

REFERENCES

1. J. R. A. Pearson, On convection cells induced by surface tension, *J. Fluid Mech.* **4,** 489–500 (1958).
2. H. Bénard, Les tourbillons cellulaires dans une nappe liquide, *Revue Gén. Sci. Pures Appliquées* **11,** 1261–1271, 1309–1328 (1901).
3. Lord Rayleigh, On the convection currents in a horizontal layer of fluid when the higher temperature is on the under side, *Phil. Mag.* **32,** 529–535 (1916).
4. D. A. Nield, Surface tension and buoyancy effects in cellular convection, *J. Fluid Mech.* **19,** 341–352 (1964).
5. J. Harvey, J. Palmer and J. C. Berg, Convective instability in liquid pools heated from below, *J. Fluid Mech.* **47,** 779–787 (1971).
6. A. Vidal and A. Acrivos, Effect of nonlinear temperature profiles on the onset of convection driven surface tension gradients, *IEC Fundamen.* **7,** 53–58 (1968).
7. J. H. Lichtenbelt, A. A. H. Drinkenburg and H. A. Dijkstra, Marangoni convection and mass transfer from the liquid gasphase, *Proc. Norderncy Symp. on Scientific Results of the German Spacelab Mission D1*, pp. 127–130. DFVLR (1987).
8. P. G. Grodzka and T. C. Bannister, Heat flow and convection demonstration experiments, *Science* **176,** 506–508 (1972).
9. P. G. Grodzka and T. C. Bannister, Heat flow and convection experiments aboard Apollo 17, *Science* **187,** 165–167 (1975).
10. P. G. Grodzka, C. Fan and R. O. Hedden, The Apollo 14 heat flow and convection demonstration experiments: final results of data analyses, LMSC-HREC D22 5333, Lockheed Missiles and Space Company (1971).
11. T. C. Bannister, P. G. Grodzka, L. W. Spradley, S. V. Bourgeois, R. O. Hedden and B. R. Facemire, Apollo 17 heat flow and convection experiments, final data analyses results, NASA TMX-64772, NASA Technical Memorandum (1973).
12. E. L. Koschmieder and M. I. Bigerstaff, Onset of surface-tension-driven Benard convection, *J. Fluid Mech.* **167,** 24–49 (1986).
13. D. Schwabe, O. Dupont, P. Queeckers and J. C. Legros, Experiments on Marangoni–Bénard instability problems, *Proc. VIIth European Symp. on Material and Fluid Sciences in Microgravity*, pp. 291–298, ESA-SP 295 (1990).
14. I. G. Currie, The effect of heating rate on the stability of stationary fluids, *J. Fluid Mech.* **29,** 337–347 (1967).
15. O. Dupont, M. Hennenberg and J. C. Legros, TEXUS 21/ESA: Bénard–Marangoni instability in a rectangular cell, pp. 36–48, ESA-SP 1132 (1992).
16. R. J. Schmidt and S. W. Milverton, On the instability of a fluid when heat from below, *Proc. R. Soc. (London) A* **152,** 586–594 (1935).

APPENDIX

We have to solve

$$(D^2-\alpha^2)g(\xi) = f(\xi)[a_1^* + 2a_2^*(\xi-1) + 3a_3^*(\xi-1)^2]$$

where $f(\xi)$ is given by equation (8). The above equation is a non-homogeneous second order ordinary differential equation whose inhomogeneous part is the sum of products of polynoms by exponentials, these last being solution of the homogeneous part. Applying a classical method, we obtain explicitly $g(\xi)$. From equation (7c), we deduce immediately the analytical value of the Marangoni parameter. As the copper wall is a thermal conductor we will consider only $g(0) = 0$ and obtain

$$g(\xi) = r[(G_1\xi^4 + G_3\xi^3 + G_5\xi^2 + G_7\xi + G_9)\sinh\alpha\xi + (G_2\xi^4 + G_4\xi^3 G_6\xi^2 + G_8\xi)\cosh\alpha\xi]$$

where

$$G_1 = -\tfrac{3}{8}a_3^*$$

$$G_2 = \frac{3}{8\alpha}a_3^*\frac{\alpha\cosh\alpha - \sinh\alpha}{\sinh\alpha}$$

$$G_3 = \frac{1}{6\alpha}[-(2a_2^* - 6a_3^*)\alpha - 12G_2]$$

$$G_4 = \frac{1}{6\alpha}\left[3a_3^* - 12G_1(2a_2^* - 6a_3^*)\frac{\alpha\cosh\alpha - \sinh\alpha}{\sinh\alpha}\right]$$

$$G_5 = \frac{1}{4\alpha}[-\alpha(a_1^* + 3a_3^* - 2a_2^*) - 6G_4]$$

$$G_6 = \frac{1}{4\alpha}\left[(a_1^* + 3a_3^* - 2a_2^*)\frac{\alpha\cosh\alpha - \sinh\alpha}{\sinh\alpha} + 2a_2^* - 6a_3^* - 6G_3\right]$$

$$G_7 = -\frac{G_6}{\alpha}$$

$$G_8 = \frac{1}{2\alpha}(a_1^* + 3a_3^* - 2a_2^* - 2G_5)$$

$$G_9(\alpha \cosh \alpha + B \sinh \alpha)$$
$$= -[(4G_1 + \alpha G_2 + 3G_3 + \alpha G_4 + 2G_5 + \alpha G_6 + G_7 + \alpha G_8) \sinh \alpha + (\alpha G_1 + 4G_2 + \alpha G_3 + 3G_4 + \alpha G_5 + 2G_6 + \alpha G_7 + G_8) \cosh \alpha - B(G_1 + G_3 + G_5 + G_7) \sinh \alpha - B(G_2 + G_4 + G_6 + G_8) \cosh \alpha].$$